Journal of Catalysis 264 (2009) 175–182

Contents lists available at ScienceDirect

Journal of Catalysis

journal homepage: www.elsevier.com/locate/jcat

Effect of substrate polarity on photocatalytic activity of titanium dioxide particles embedded in mesoporous silica

Yasuhiro Shiraishi *, Yoshitsune Sugano, Daisuke Inoue, Takayuki Hirai

Research Center for Solar Energy Chemistry, and Division of Chemical Engineering, Graduate School of Engineering Science, 1-3 Machikaneyama-cho, Osaka University, Toyonaka 560-8531, Japan

ARTICLE INFO

Article history:
Received 4 December 2008
Revised 25 March 2009
Accepted 1 April 2009
Available online 7 May 2009

Keywords:
Mesoporous silica
Titanium dioxide
Photocatalyst
Hydroxyl radical
Selective organic transformation
Phenol synthesis

ABSTRACT

Photocatalytic activity of TiO_2 particles embedded in mesoporous silica (TiO_2@MPS), prepared by surfactant-templating method with a TiO_2 colloidal suspension, has been studied in water with molecular oxygen. Photocatalytic reactions of several kinds of aromatic molecules with TiO_2@MPS reveal that less polar substrates show high reactivity, while polar substrates show much lower reactivity. Electron spin resonance analysis with spin-trapping reagents reveals that less polar substrates diffuse easily into the pore of the catalysts and react efficiently with short-lived hydroxyl (·OH) radicals formed at the surface of inner TiO_2 particles, resulting in a high reactivity. In contrast, polar substrates cannot diffuse into the pores and hence, shows a low reactivity. The photocatalytic activity of TiO_2@MPS driven by the substrate polarity is applicable to selective transformation of a less polar reactant to a polar product, such as hydroxylation of benzene to phenol with high selectivity (>69%).

1. Introduction

Development of highly selective methods for photochemical organic synthesis is one of the biggest challenges in chemistry. Photocatalytic organic synthesis with a heterogeneous catalyst is particularly attractive for practical applications because of the ease of catalyst recovery. Much investigation has been carried out with a semiconductor titanium dioxide (TiO_2) [1–6]. In most cases, photocatalytic reactions on TiO_2 in water proceed via following steps [7–9]: (i) generation of excited electron (e^-)–positive hole (h^+) pairs by absorption of supra-bandgap photons, (ii) production of hydroxyl radicals (·OH) via reaction of h^+ with surface –OH groups or adsorbed H_2O molecules, and (iii) oxidation of substrates by ·OH. Oxidation by ·OH is, however, nonselective, resulting in insufficient product selectivity. Development of photocatalytic systems enabling selective organic transformations, especially in water, continues to be studied intensively by many researchers [10–13].

Up to now, only a few systems of selective photocatalytic reactions on TiO_2 in water have been reported [14–17], where the size of substrates and the affinity of substrates with the catalyst surface are the important factors for selective transformation. Recently, Inumaru et al. have reported a new photocatalytic system employing TiO_2 particles embedded in mesoporous silica (TiO_2@MPS), easily synthesized by the hydrolysis of silica source in the presence of TiO_2 particles [18]. Competitive reaction experiments with alkyl-substituted phenols (phenol, 4-*n*-propylphenol, 4-*n*-heptylphenol, and 4-nonylphenol) reveal that the TiO_2@MPS catalyst promotes preferential decomposition of less polar 4-*n*-heptylphenol and 4-nonylphenol, while keeping the reactivity of polar phenol and 4-*n*-propylphenol low. The interesting catalytic property is explained by the higher affinity of less polar substrates with the inner MPS surface, leading to their enhanced decomposition at the surface of inner TiO_2 particles. Besides the interesting properties of TiO_2@MPS, detailed photocatalytic mechanism remains to be clarified. Recently, similar MPS materials containing TiO_2 particles have been synthesized [19–24]; however, in none of the reports, the mechanism of selective photocatalytic reactions has been studied.

The purpose of this work is the application of TiO_2@MPS catalysts to selective organic transformation. We first studied the detailed photocatalytic activity of $x$$TiO_2$@MPS catalysts ($x$ (wt%) = Ti/(Ti + Si) × 100; x = 29, 40, 57, 76) to clarify the catalytic mechanism. Reactivity tests with several kinds of benzene derivatives and electron spin resonance (ESR) analysis revealed that the catalytic activity of $x$$TiO_2$@MPS depends strongly on the polarity of substrates and on the behavior of ·OH within MPS; less polar substrates can enter into the pore of MPS easily and can react efficiently with short-lived ·OH formed at the surface of inner TiO_2 particles, promoting preferential reaction of less polar substrates. We also found that the catalytic activity of $x$$TiO_2$@MPS, which is driven by the substrate polarity, is applicable to selective transformations of less polar reactants to polar products, such as selective transformation of benzene to phenol (>69%).

* Corresponding author.
E-mail address: shiraish@cheng.es.osaka-u.ac.jp (Y. Shiraishi).

0021-9517/$ - see front matter © 2009 Elsevier Inc. All rights reserved.
doi:10.1016/j.jcat.2009.04.001

2. Experimental

2.1. Materials

All the reagents used were of the highest commercial quality, which were supplied from Wako, Tokyo Kasei, and Aldrich, and were used without further purification. Water was purified by the Milli Q system. xTiO$_2$@MPS catalysts [x (wt%) = Ti/(Ti + Si) × 100; x = 0, 29, 40, 57, 76] were synthesized according to the literature procedure [24] as follows: $TiCl_4$ (3.1 g, 16.5 μmol) and H_2SO_4 (1.4 g) were added to water (100 ml) and stirred at 273 K for 30 min and at room temperature for 30 min. Required amount of water glass ($Na_2SiO_3 \cdot H_2O$, 2 mol l^{-1} aqueous solution) was added to the solution and the mixture was stirred at room temperature, where pH of the solution was adjusted to 2.0 by adding an aqueous $(NH_4)_2CO_3$ solution (0.3 mol l^{-1}). Cetyltrimethyl ammonium bromide (CTAB; 33 g) was added to the mixture and stirred at 363 K for 48 h. The resulting solid was recovered by filtration, washed thoroughly with water and ethanol, and dried at 373 K for 24 h. The resultant was calcined at 753 K for 2 h under air flow. The feed amounts of $TiCl_4$ and water glass and the properties of the respective catalysts are summarized in Table 1.

2.2. Photoreaction

Each catalyst (10 mg) was suspended in a buffered aqueous solution (pH 7; 10 ml; consisting of 0.05 M KH_2PO_4 and 0.03 M NaOH) containing each substrate within a Pyrex glass tube (ϕ 10 mm; capacity, 20 cm^3). The tube was sealed using a rubber septum cap, and O_2 was bubbled slowly through the solution for 5 min in an ice bath to avoid the evaporation of substrates, where the substrate concentrations do not change during this process. The sample was photoirradiated by magnetic stirring using a high-pressure Hg lamp (300 W; Eikohsha Co, Ltd., Osaka) [25–27], filtered through an uranil glass to give light wavelengths of λ > 320 nm. The light intensity was 9.0 mW m^{-2} (at 320–420 nm), and the temperature of the solution during photoirradiation was 313 K. The gas phase was analyzed by GC-TCD (Shimadzu; GC-8A) to determine the CO_2 amount. The liquid phase was recovered by centrifugation, and the resulting catalyst was washed with acetonitrile. The combined solution was analyzed by a reverse-phase HPLC (Shimadzu LC-6A) equipped with UV–vis spectrometric detector (Shimadzu SPD-6A; λ_{abs} = 254 nm) or GC-FID (Shimadzu; GC-1700) to determine the amount of substrates and products.

2.3. Analysis

ESR spectra were recorded at the X-band using a Bruker EMX-10/12 spectrometer with a 100 kHz magnetic field modulation at a microwave power level of 1.0 mW, where the microwave power saturation of the signals does not occur [28,29]. The magnetic field was calibrated using a 1,1′-diphenyl-2-picrylhydrazyl (DPPH) as a standard. Catalyst (10 mg) and buffered aqueous solution (pH 7; 20 μl) containing respective spin-trapping reagent (5 mM) were introduced to a flat quartz cell [5 mm × 20 mm × 0.5 mm (path length)]. The cell was placed on an ESR sample cavity, and the measurement was started under photoirradiation with 500 W Xe lamp (USHIO Inc.; λ > 300 nm). Powder XRD analysis (Cu Kα radiation) was performed with a Philips XXX diffractometer [30]. Diffuse reflectance UV–vis spectra were measured on a UV–vis spectrophotometer (Jasco Corp.; V-550 with integrated sphere apparatus ISV-469) [31,32]. N_2 adsorption/desorption measurements were performed at 77 K using an AUTOSORB-1-C/TCD analyzer (Yuasa Ionics Co., Ltd.). A polarity parameter, logS (Logarithm of solubility in water), for substrates was calculated on the basis of the ALOGPS 2.1 program on the web site (http://www.vcclab.org/lab/alogps) [33,34].

3. Results and discussion

3.1. Catalyst properties

xTiO$_2$@MPS catalysts [x = 29, 40, 57, and 76] were synthesized by surfactant-templated hydrolysis of Na_2SiO_3 in a TiO$_2$ colloidal suspension [24]. Table 1 summarizes the properties of catalysts. As shown in Fig. 1a, powder XRD patterns of all catalysts show d_{100} diffraction at 1.0–3.0°. As shown in Fig. 2, N_2 adsorption/desorption analysis of these catalysts shows type IV isotherm and the presence of 2–5 nm pores. These data indicate that, as reported in [24], xTiO$_2$@MPS catalysts contain mesopores. As shown in Table 1, particle size of the catalysts decreases with a decrease in Si content; 29TiO$_2$@MPS has 9.4 μm diameter, whereas 76TiO$_2$@MPS has only 2.0 μm. This is probably because lower amount of silica source (Na_2SiO_3) suppresses the silica aggregation, leading to the formation of smaller catalyst particles. The size of TiO$_2$ particles within the catalysts is then determined by laser scattering analysis after washing the catalysts with an aqueous KOH (1 mol l^{-1}) solution. As shown in Fig. 3, the size of TiO$_2$ particles within x = 29, 40, and 55 catalysts (a–c) is almost unchanged (0.16–0.17 μm). This is because the same amount of colloidal

Table 1
Properties of xTiO$_2$@MPS catalysts.

Catalyst	Feed amount		Ti (wt%)[b]	Catalyst particle size (μm)[c]	A_{BET} (m^2 g^{-1})[d]	D_p (nm)[e]	E_{bg} (eV)[f]	TiO$_2$ particle size (μm)[g]
	$TiCl_4$ (μmol)	Water glass (g)[a]						
0TiO$_2$@MPS		50	0	18.5	825	5.09		
29TiO$_2$@MPS	16.5	34.2	29	9.37	910	3.13	3.49	0.16
40TiO$_2$@MPS	16.5	20.5	40	7.50	788	2.99	3.56	0.17
57TiO$_2$@MPS	16.5	10.3	57	6.76	709	2.82	3.35	0.17
76TiO$_2$@MPS	16.5	4.3	76	2.02	269	3.68	3.37	0.49
TiO$_2$ (anatase)			100	5.5	49		3.34	5.5

[a] Aqueous Na_2SiO_3 solution (2 mol l^{-1}).
[b] =Ti/(Ti + Si) × 100. The composition was determined by inductively coupled argon plasma atomic emission spectrometer (ICAP-AES).
[c] Determined by static laser scattering analysis. The detailed size distribution data are shown in Fig. 3.
[d] BET surface area.
[e] Average pore diameter determined by DH method.
[f] Measured by a plot of the Kubelka–Munk function versus the energy of light adsorbed (Fig. 4).
[g] Determined by dynamic laser scattering analysis after washing the catalysts with an aqueous KOH solution (1 mol l^{-1}). The detailed size distribution data are shown in Fig. 3.

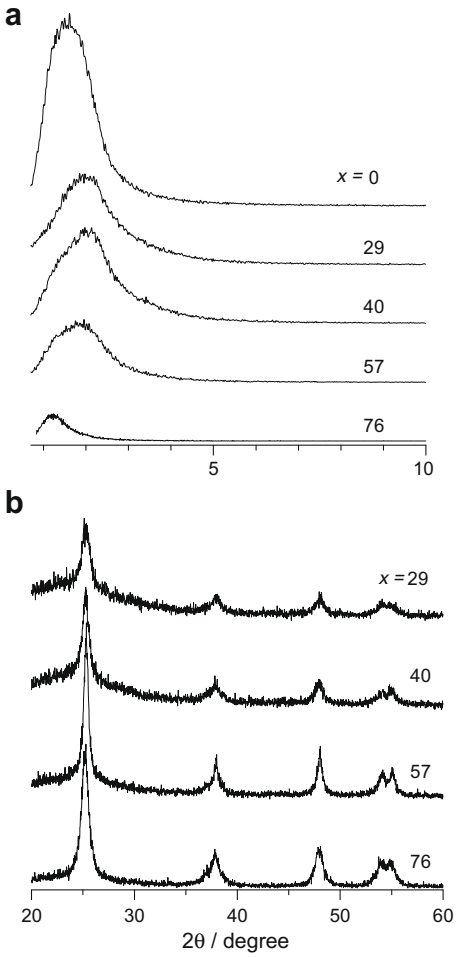

Fig. 1. (a) Low-angle and (b) high-angle powder XRD patterns of xTiO$_2$@MPS catalysts.

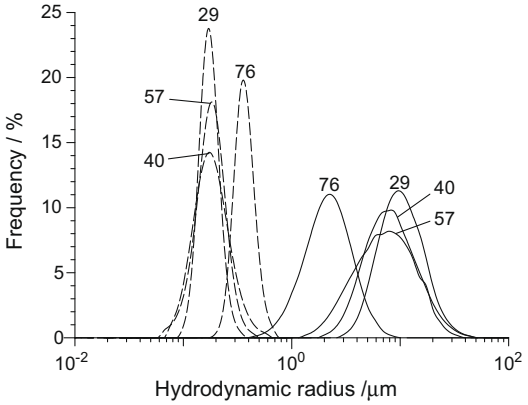

Fig. 3. Size distributions of (solid line) catalyst particles and (dotted line) inner TiO$_2$ particles for xTiO$_2$@MPS. The numbers in the figure denote x.

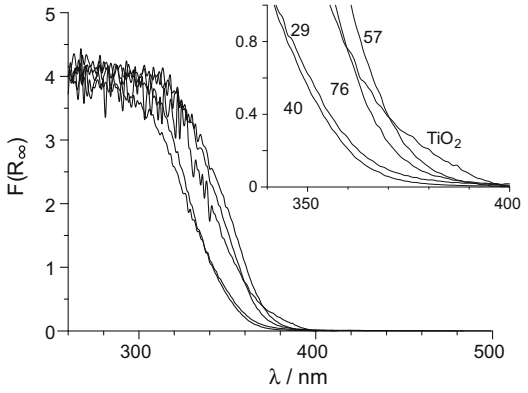

Fig. 4. Diffuse reflectance UV–vis spectra of the respective catalysts. The numbers in the figure denote x of the respective xTiO$_2$@MPS catalysts.

TiO$_2$ suspension is used for catalyst synthesis. However, x = 76 catalyst (d) contains larger TiO$_2$ particles (0.49 μm). In this catalyst, Ti amount is much higher than the Si amount and hence, the TiO$_2$ particles are located closely to one other. Calcination of the catalysts, therefore, leads to sintering of the TiO$_2$ particles, resulting in the formation of large TiO$_2$ particles. As shown in Fig. 1b, high-angle powder XRD patterns of xTiO$_2$@MPS catalysts reveal that TiO$_2$ particles within all the catalysts have anatase structure. This is consistent with the data reported previously [24]. Band gap energies determined by diffuse reflectance UV–vis spectra of xTiO$_2$@MPS catalysts (Fig. 4) are 3.35 to 3.36 eV, which are higher than those of bulk anatase TiO$_2$ (3.34 eV). This is because the Si–O–Ti bond forms at the interface between the TiO$_2$ particles and the silica phase [24]. The Si–O–Ti bond formation is confirmed by IR

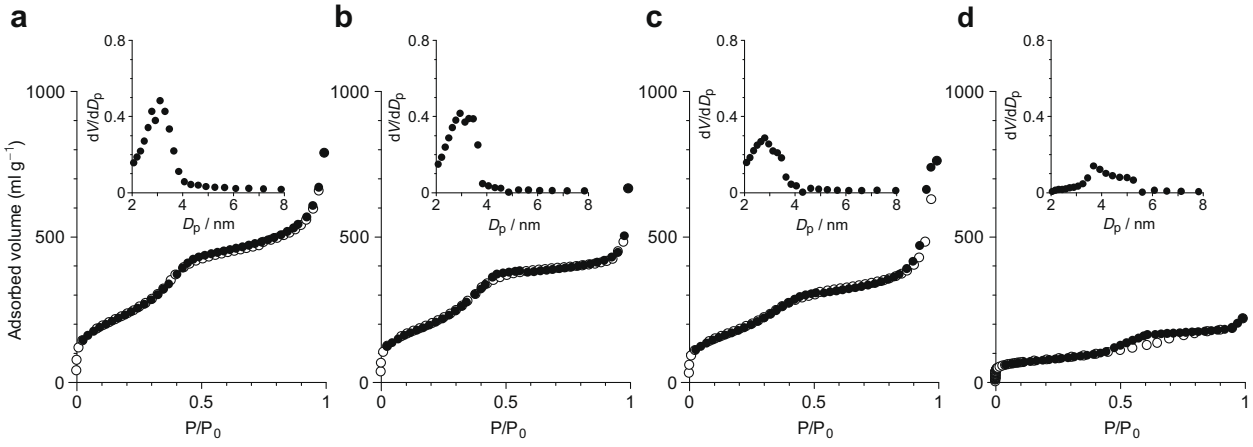

Fig. 2. N_2 adsorption (closed symbols)/desorption (open symbols) isotherm and (inset) pore size distribution of the respective catalysts: (a) 29TiO$_2$@MPS, (b) 40TiO$_2$@MPS, (c) 57TiO$_2$@MPS, and (d) 76TiO$_2$@MPS.

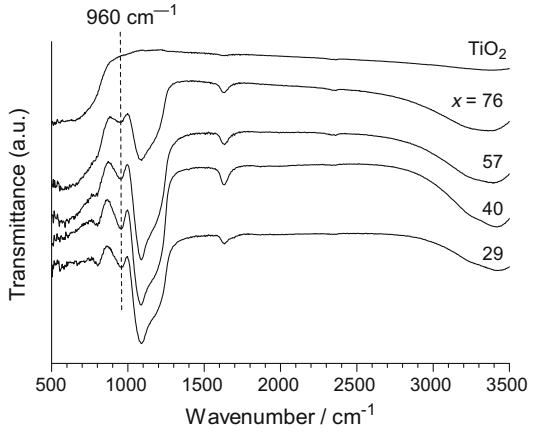

Fig. 5. FT-IR spectra of TiO_2 and xTiO$_2$@MPS catalysts.

Table 2
The logS values of the respective substrates and spin-trapping agents[a].

	logS
Benzene	−1.85
Toluene	−2.26
Chlorobenzene	−2.77
Phenol	−0.31
Hydroquinone	−0.06
Catechol	−0.17
Nitrosobenzene (NB)	−2.08
α-Phenyl-*N*-*tert*-butylnitrone (PBN)	−1.30

[a] Determined by the ALOGPS 2.1 program [33,34].

absorption. As shown in Fig. 5, the xTiO$_2$@MPS catalysts show distinctive absorption at 960 cm^{-1}, assigned to the Si–O–Ti bond [24].

3.2. Photocatalytic activity

The photocatalytic activity of xTiO$_2$@MPS catalysts was studied with six kinds of benzene derivatives as substrates (benzene, toluene, chlorobenzene, phenol, hydroquinone, and catechol) in buffered aqueous solution (pH 7) with molecular oxygen. To clarify the effects of substrate polarity on reactivity, a polarity parameter, logS (logarithm of solubility in water), was calculated on the basis of the ALOGPS 2.1 program developed by Tekto et al. [33,34]. The logS values of the respective substrates are summarized in Table 2, where a more negative value indicates a lower polarity and a poorer water solubility [17,35,36]. The first three substrates (benzene, toluene, and chlorobenzene) have more negative logS values (<−1.8) than do the other three substrates (phenol, hydroquinone, and catechol) (>−0.3), so that the two groups can be classified as less polar substrates and polar substrates, respectively [17]. To clarify the relationship between the reactivity of substrates and their adsorption behavior onto the catalyst surface, the degree of substrate adsorption onto the catalyst was defined as the distribution ratio, K_D, as follows [16]:

$$K_D = (C_0 - C_e)/C_e \quad (1)$$

where C_0 denotes the initial concentration of substrate in solution and C_e denotes the equilibrium concentration of substrate in the solution after 0.5 h of stirring with the respective catalysts at 313 K. It is noted that all the samples attain the adsorption equilibrium within 0.5 h under this condition. Fig. 6A summarizes the K_D values obtained by the respective catalysts. On both TiO_2 and xTiO$_2$@MPS, less polar substrates (benzene, toluene, and

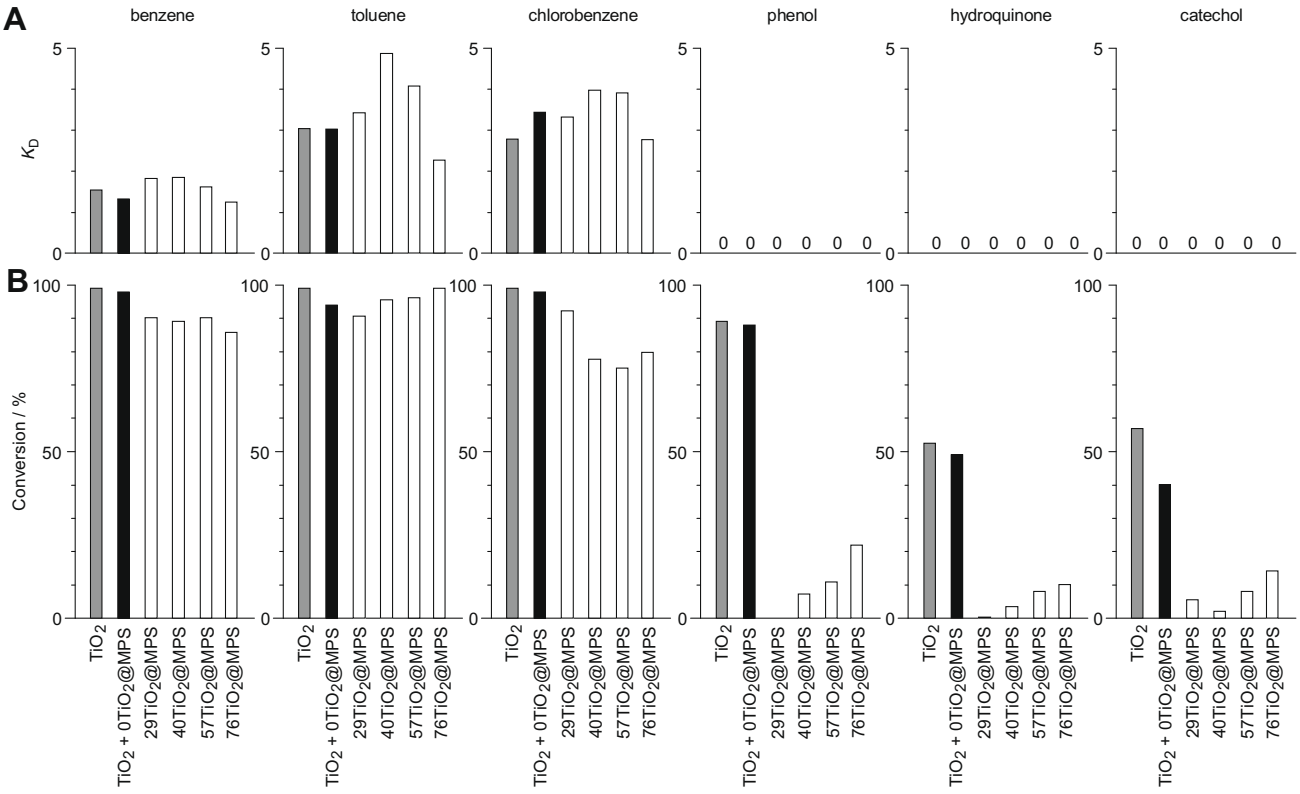

Fig. 6. (A) Distribution ratio, K_D, and (B) conversion of substrates on the respective catalysts during photoirradiation ($\lambda > 320$ nm, 2 h). Reaction conditions are buffered aqueous solution (10 ml, pH 7), substrate (2 mM), catalyst (10 mg), O_2 (1 atm). The K_D is defined in Eq. (1).

chlorobenzene) show high K_D values (>1), whereas the values of the polar substrates (phenol, hydroquinone, and catechol) are almost zero. These data clearly indicate that less polar substrates are adsorbed strongly onto the surface of both TiO_2 and xTiO$_2$@MPS. Fig. 6B shows conversion of substrates on the respective catalysts under photoirradiation at $\lambda > 320$ nm. On TiO_2, conversions of less polar substrates are very high (>90%), and polar substrates also show high conversions (>50%). In contrast, on xTiO$_2$@MPS catalysts, the less polar substrates still show high conversion (>75%), but the polar substrates show very low conversion (<20%). These data clearly suggest that on xTiO$_2$@MPS, less polar substrates that have strong affinity with the catalyst surface react efficiently, whereas polar substrates that have poor affinity with the catalyst surface show low reactivity. The results are consistent with that reported previously [18].

The polarity-driven photocatalytic activity of xTiO$_2$@MPS is explained as follows: less polar substrates have strong affinity with the inner MPS and TiO_2 surfaces. The concentration of these substrates within the pore, therefore, becomes higher than that in bulk water, resulting in high reactivity. In contrast, polar substrates have poor affinity with both MPS and TiO_2 surfaces. The concentration of these substrates within the catalyst pore, therefore, becomes lower than that in bulk water, resulting in low reactivity. As shown in Fig. 6A, adsorption behavior of substrates on bulk TiO_2 is similar to that on xTiO$_2$@MPS; less polar substrates are scarcely adsorbed onto bulk TiO_2, as is also the case for xTiO$_2$@MPS. The conversion of polar substrates on bulk TiO_2 is, however, much higher than that on xTiO$_2$@MPS (Fig. 6B). This may be because the surface of bulk TiO_2 faces the bulk solution, enabling the reaction of polar substrates to result in high conversion. These imply that the MPS parts of the xTiO$_2$@MPS catalysts behave as a filter to allow selective diffusion of less polar substrates. To clarify the effect of the MPS parts on the catalytic activity, a mechanical mixture of 0TiO$_2$@MPS and bulk TiO_2 was used for reaction. As shown in Fig. 6 (gray bars), polar substrates are scarcely adsorbed onto the catalyst surface, as is the case for xTiO$_2$@MPS. However, the conversion of polar substrates is higher, as is the case for bulk TiO_2. This supports the above assumption: the polarity-driven photocatalytic activity of xTiO$_2$@MPS arises from the filtering effect by the MPS parts.

3.3. ·OH behavior

The above findings indicate that, on xTiO$_2$@MPS catalysts, less polar substrates can enter into the pore easily and react efficiently. In contrast, polar substrates cannot enter into the pore, resulting in low reactivity. It is necessary to further clarify the selective catalytic mechanism on xTiO$_2$@MPS. In both xTiO$_2$@MPS and bulk TiO_2 systems, addition of D-mannitol (100 mM; 50 equiv of substrate), a typical hydroxyl radical (·OH) scavenger [16,17], completely suppresses the reaction of all substrates. This indicates that, on xTiO$_2$@MPS, ·OH formed at the surface of TiO_2 particles within MPS behaves as the active species.

An important question that must be addressed first is whether the ·OH formed at the surface of TiO_2 particles within MPS can diffuse out to bulk water. As described in [37], ·OH reacts with an inorganic surface, such as TiO_2 and SiO_2, and is converted to inactive surface –OH group at a near-diffusion controlled rate. The rate equation can be expressed as follows:

$$-\frac{d[\cdot OH]}{dt} = k_{\cdot OH} A' [\cdot OH] \tag{2}$$

where $k_{\cdot OH}$ is the rate constant per unit surface area of inorganic material (l m^{-2} s^{-1}), A' is the surface area of the inorganic material per unit volume of water (m^2 l^{-1}), and [·OH] is the ·OH concentration (mol l^{-1}). As described [37], $k_{\cdot OH}$ for reaction of ·OH with TiO_2 surface is determined to be 1.8×10^3 l m^{-2} s^{-1} at ambient temperature. As reported in [38], ·OH reacts with SiO_2 ten times faster than with TiO_2; therefore, $k_{\cdot OH}$ for reaction of ·OH with SiO_2 surface is determined to be ca. 1.8×10^4 l m^{-2} s^{-1}. To clarify whether the ·OH formed at the surface of TiO_2 particles within MPS can diffuse out to bulk solution or not, the lifetime and diffusion distance of ·OH, when existing inside a cylindrical SiO_2 wall of MPS, were determined. The surface area of the SiO_2 wall per unit pore volume of MPS can be expressed as Eq. (3), based on the pore volume, V_p, and internal surface area, A_{int}, of MPS. In this, A_{int} is roughly estimated by subtracting the external surface area (A_{ext}) from the BET surface area (A_{BET}) [16], as shown in Table 3.

$$A' = \frac{A_{int}}{V_p} = \frac{A_{BET} - A_{ext}}{V_p} \tag{3}$$

The lifetime of ·OH within the pore of MPS, τ, can be expressed as Eq. (4), where τ is the time constant for the ·OH decay, which is defined as the period to attain the e^{-1} value of the magnitude of whole change of [·OH].

$$\tau = \frac{1}{k_{\cdot OH} A'} \ln\left(\frac{[\cdot OH]_t}{[\cdot OH]_0}\right) = \frac{1}{k_{\cdot OH} A'} \ln(e^{-1}) = \frac{1}{k_{\cdot OH} A'} \tag{4}$$

The diffusion distance of ·OH within its lifetime, x, can be roughly estimated with an empirical equation using diffusion coefficient and time, as follows [39],

$$x = \sqrt{D_{\cdot OH}\tau} \tag{5}$$

where $D_{\cdot OH}$ is the diffusion coefficient of ·OH in water ($=2.6 \times 10^{-9}$ m^2 s^{-1}) at ambient temperature [40]. The lifetime of ·OH and its diffusion distance within the pore of the catalysts are 0.07 to 0.28 ns and 0.43 to 0.85 nm, respectively. The diffusion distance is much smaller than the pore diameter of MPS (<6 nm). This suggests that most of the ·OH formed at the surface of TiO_2 particles within MPS scarcely diffuse out of the pores. These results clearly support the proposed reaction mechanism: polar substrates that exist outside the pores of MPS scarcely react with ·OH that is formed, whereas less polar substrates that can enter into the pore of MPS react efficiently with ·OH.

3.4. ESR analysis

To further confirm the catalytic mechanism of xTiO$_2$@MPS involving ·OH, ESR analysis for ·OH was carried out with two kinds

Table 3
Calculated lifetime of ·OH (τ) and its diffusion distance (x) within the lifetime on TiO$_2$@MPS catalysts.

Catalyst	A_{BET}(m^2 g^{-1})[a]	A_{ext} (m^2 g^{-1})[b]	A_{int} (m^2 g^{-1})[c]	V_p (mm^3 g^{-1})[d]	τ (ns)	x (nm)
29TiO$_2$@MPS	910	257	653	1220	0.21	0.74
40TiO$_2$@MPS	788	92	696	1030	0.07	0.43
57TiO$_2$@MPS	709	189	520	1178	0.28	0.85
76TiO$_2$@MPS	269	41	228	338	0.08	0.46

[a] BET surface area.
[b] External surface area determined by the t-plot volumetric measurements with N_2.
[c] $= A_{BET} - A_{ext}$.
[d] Pore volume.

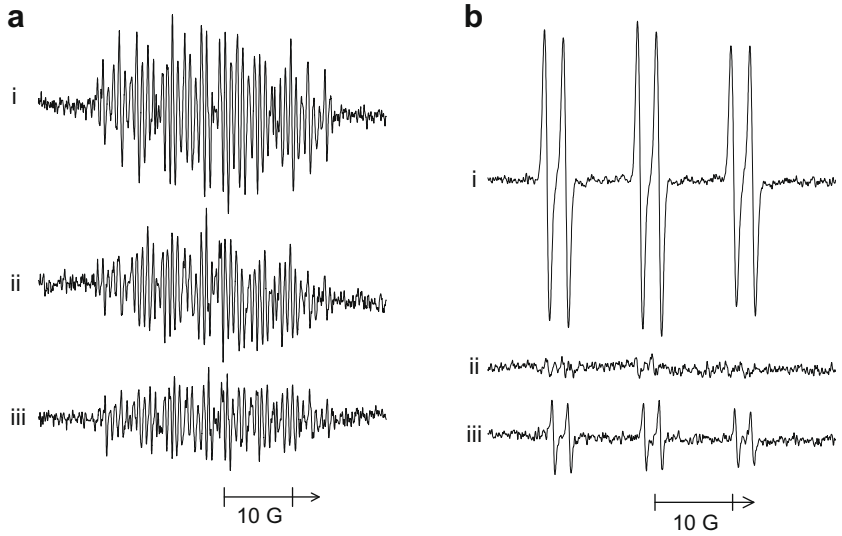

Fig. 7. ESR spectra of ·OH spin adduct signals obtained under photoirradiation of a buffered aqueous solution containing the respective spin-trapping agent, (a) NB and (b) PBN, in the presence of (i) TiO_2 (anatase), (ii) 40TiO_2@MPS, and (iii) 76TiO_2@MPS.

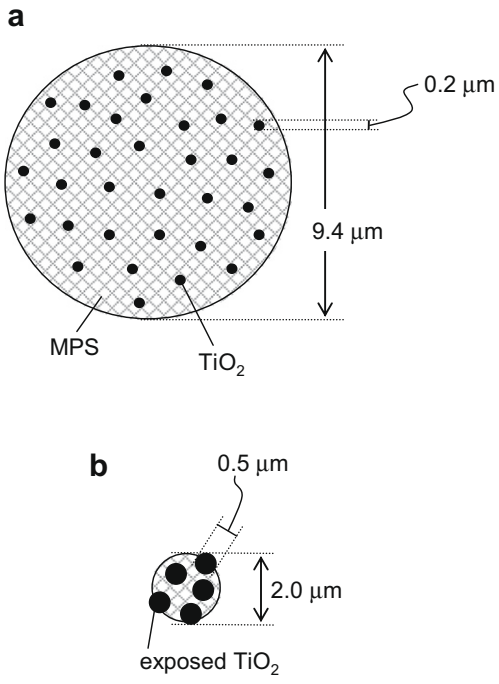

Fig. 8. Schematic representation of (a) 29TiO_2@MPS and (b) 76TiO_2@MPS catalysts.

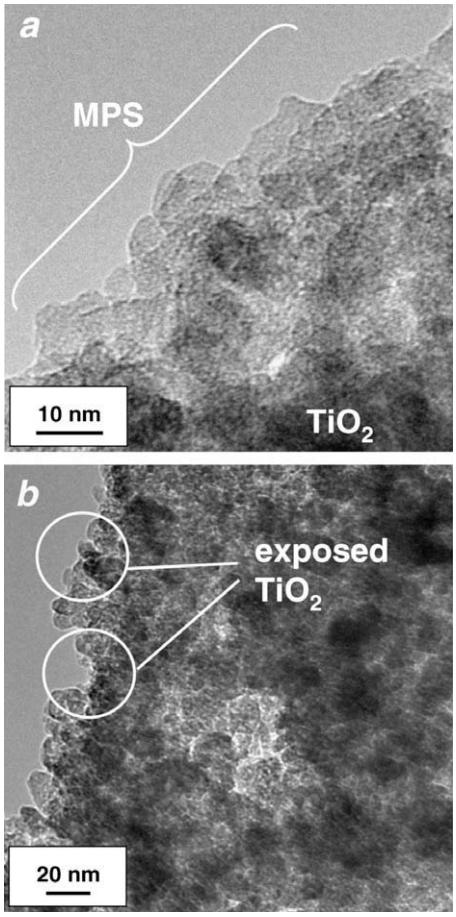

Fig. 9. TEM images of (a) 29TiO_2@MPS and (b) 76TiO_2@MPS catalysts.

of spin-trapping agents, nitrosobenzene (NB) [41,42], and α-phenyl-*N*-*tert*-butylnitrone (PBN) [43]. As shown in Table 2, logS of NB (−2.08) is more negative than that of PBN (−1.30). Comparison of the logS values of NB and PBN with those of substrates indicates that NB is classified as a less polar substrate, while PBN is classified as a polar substrate. Adsorption experiments with the spin-trapping agents confirm this; K_D values of NB on bulk TiO_2 and *x*TiO_2@MPS catalysts are relatively high (>0.5), whereas the values of PBN are zero. The respective spin-trapping agents were dissolved in a buffered aqueous solution (pH 7) together with bulk TiO_2 or *x*TiO_2@MPS, and ESR analysis was carried out under photoirradiation. Fig. 7a shows ESR spectra of the sample containing NB. As shown in spectrum (i), photoirradiation of bulk TiO_2 shows distinctive NB–·OH spin adduct signals [41,42]. In the case of 40TiO_2@MPS (ii), similar signals appear although at a decreased intensity level, indicating that reaction of ·OH with less polar NB occurs on this catalyst. The ESR data are consistent with the reactivity data for less polar substrates (Fig. 6); NB can enter into the pore of *x*TiO_2@MPS; hence, it reacts efficiently with ·OH. In the case of PBN (Fig. 7b), bulk TiO_2 (i) shows distinctive PBN–·OH spin

Table 4
Photocatalytic transformation of benzene to phenol[a].

Run	Catalyst	Photoirradiation time (h)	Yield (μmol)			Phenol selectivity (%)[c]
			Phenol	Others[b]	CO_2	
1	TiO_2 (anatase)	4	3.1	7.9	4.9	26
2	TiO_2 (anatase)	10	16.0	38.4	23	27
3	29TiO_2@MPS	10	2.8	0.6	0.4	81
4	40TiO_2@MPS	10	3.4	0.7	0.5	81
5	57TiO_2@MPS	10	3.5	1.1	1.1	73
6	76TiO_2@MPS	10	4.6	1.8	1.5	69
7	40TiO_2@MPS	20	10.7	1.8	13	73
8	40TiO_2@MPS	30	20.1	3.4	22	74

[a] Reaction conditions are $\lambda > 320$ nm; benzene, 0.5 ml; buffered (pH 7) aqueous solution, 4.5 ml; catalyst, 10 mg; temperature, 313 K; O_2, 1 atm.
[b] The sum of the yields of hydroquinone, catechol, resorcinol, and benzoquinone.
[c] =[phenol]/([phenol] + [others] + [CO_2]/6) × 100.

adduct signals [43]. In contrast, 40TiO_2@MPS (ii) shows no adduct signal, indicating that polar PBN does not react with ·OH. The ESR results indicate that polar PBN cannot enter into the pore of $x$$TiO_2$@MPS and scarcely reacts with ·OH; the result agrees with the reactivity data (Fig. 6). The above ESR results clearly support our assumption: on $x$$TiO_2$@MPS, less polar substrates can enter into the pore and, hence, react efficiently with ·OH. In contrast, polar substrates have poor affinity to the pore wall and TiO_2 particles and, hence, cannot enter into the pore of the catalysts, resulting in very low reactivity with ·OH.

As shown in Fig. 6, reactivity of less polar substrates with all $x$$TiO_2$@MPS catalysts (c–f) is similar. However, the reactivity of polar substrates increases with increase in the amount of Ti; for example, the conversion of phenol on 29TiO_2@MPS is almost zero, but the conversion on 76TiO_2@MPS is 22%. The higher conversion of polar substrates on 76TiO_2@MPS catalyst is due to the larger amount of TiO_2 particles. These particles are insufficiently embedded within the MPS phase, and parts of the TiO_2 particles are exposed on the catalyst surface, as schematically shown in Fig. 8. The exposed TiO_2 particles may, therefore, even enhance the reaction with polar substrates in bulk water, resulting in a high conversion of polar substrates. This is confirmed by TEM images of the catalysts. As shown in Fig. 9a, in the case of 29TiO_2@MPS catalyst, TiO_2 particles are sufficiently surrounded by MPS phase. However, in the case of 76TiO_2@MPS catalyst (Fig. 9b), parts of the TiO_2 particles are exposed on the catalyst surface. This supports the exposed structure of the catalysts with larger TiO_2 content. This is also confirmed by ESR analysis. As shown in Fig. 7b.ii, the polar PBN does not show spin-adduct signals on 40TiO_2@MPS. However, as shown in Fig. 7b.iii, 76TiO_2@MPS shows distinctive spin-adduct signals. These findings clearly suggest that, as shown in Fig. 8, $x$$TiO_2$@MPS catalysts with high TiO_2 amount contain TiO_2 particles that are exposed on the external surface of the catalysts, thus even promoting the reaction of polar substrates.

3.5. Selective photocatalytic transformation

The photocatalytic activity of $x$$TiO_2$@MPS, which is driven by the substrate polarity, is applicable to selective organic transformation. In this system, less polar substrates react efficiently, while polar substrates are inactive. This catalytic property is applicable to selective organic transformation of a less polar reactant to a polar product, enabling selective hydroxylation of benzene to phenol (Table 4). As shown in runs 1 and 2, photoirradiation of benzene on bulk TiO_2 gives rise to phenol as an initial product, but the selectivity is quite low (<27%). This is because phenol is sequentially oxidized by ·OH to form further hydroxylated products (hydroquinone, catechol, resorcinol, and benzoquinone), and is eventually decomposed completely to CO_2 [44,45]. In contrast, $x$$TiO_2$@MPS (runs 3 to 8) affords phenol with a very high selectivity (>69%). As shown in Table 2, benzene is a less polar molecule, but phenol is highly polarized. Sequential decomposition of phenol is therefore suppressed, resulting in high phenol selectivity.

As shown in Table 4 (runs 3 and 4), $x$$TiO_2$@MPS catalysts with lower Ti amount (29TiO_2@MPS and 40TiO_2@MPS) show the highest phenol selectivity, where the selectivity decreases with an increase in the Ti amount of the catalysts (runs 5 and 6). This is because, as shown in Fig. 8b, $x$$TiO_2$@MPS with high Ti content contains TiO_2 particles exposed on the external surface and, hence, allows sequential reaction of phenol. These results suggest that $x$$TiO_2$@MPS with low Ti amounts is suitable for selective phenol production. As shown in runs 7 and 8, prolonged photoirradiation does not show decrease in the phenol selectivity. Various TiO_2 systems have been applied to the photocatalytic transformation of benzene to phenol [46–50]; however, their selectivities are quite low (<21%). It is well known that phenol synthesis is currently carried out industrially via a multi-step cumene process, but the process suffers from low selectivity, high energy consumption, and formation of large quantity of byproducts. The present $x$$TiO_2$@MPS system exhibits significant advantages: (i) additive free, (ii) cheap source of oxidant (H_2O), and (iii) mild reaction condition (room temperature). Applying the basic concept presented here may help to enable phenol production in an economically and environmentally friendly way.

4. Conclusions

Photocatalytic activity of TiO_2 particles embedded in mesoporous silica ($x$$TiO_2$@MPS) has been studied in water. The $x$$TiO_2$@MPS catalysts show higher catalytic activity for reaction of less polar substrates, while showing lower activity for polar substrates. The polarity-driven photocatalytic activity of $x$$TiO_2$@MPS is applicable to the selective transformation of a less polar reactant to a polar product, enabling hydroxylation of benzene to phenol with high selectivity (>69%). The highest phenol selectivity is obtained with $x$$TiO_2$@MPS catalysts with lower amount of TiO_2 particles, which successfully suppresses sequential decomposition of phenol.

Acknowledgments

This work was supported by the Grant-in-Aids for Scientific Research (No. 20360359) from the Ministry of Education, Culture, Sports, Science, and Technology, Japan (MEXT). We are also grateful to the Division of Chemical Engineering for the Lend-Lease Laboratory System.

References

[1] A.J. Bard, J. Phys. Chem. 86 (1982) 172.
[2] M.A. Fox, M.T. Dulay, Chem. Rev. 93 (1993) 341.

[3] M.A. Fox, Acc. Chem. Res. 16 (1983) 314.
[4] A. Maldotti, A. Molinari, R. Amadelli, Chem. Rev. 102 (2002) 3811.
[5] A. Mills, S. Le Hunte, J. Photochem. Photobiol. A: Chem. 108 (1997) 1.
[6] A. Fujishima, T.N. Rao, D.A. Tryk, J. Photochem. Photobiol. C: Photochem. Rev. 1 (2000) 1.
[7] J.-M. Herrmann, Top. Catal. 34 (2005) 49.
[8] K. Hashimoto, H. Irie, A. Fujishima, Jpn. J. Appl. Phys. 44 (2005) 8269.
[9] T. Tachikawa, M. Fujitsuka, T. Majima, J. Phys. Chem. C 111 (2007) 5259.
[10] B. Ohtani, B. Pal, S. Ikeda, Catal. Surv. Asia 7 (2003) 165.
[11] G. Palmisano, V. Augugliaro, M. Pagliaro, L. Palmisano, Chem. Commun. (2007) 3425.
[12] M. Fagnoni, D. Dondi, D. Ravelli, A. Albini, Chem. Rev. 107 (2007) 2725.
[13] Y. Shiraishi, T. Hirai, J. Photochem. Photobiol. C: Photochem. Rev. 9 (2008) 157.
[14] S. Ghosh-Mukerji, H. Haick, M. Schvartzman, Y. Paz, J. Am. Chem. Soc. 123 (2001) 10776.
[15] P. Calza, C. Pazé, E. Pelizzetti, A. Zecchina, Chem. Commun. (2001) 2130.
[16] Y. Shiraishi, N. Saito, T. Hirai, J. Am. Chem. Soc. 127 (2005) 12820.
[17] Y. Shiraishi, D. Tsukamoto, T. Hirai, Langmuir 24 (2008) 12658.
[18] K. Inumaru, T. Kasahara, M. Yasui, S. Yamanaka, Chem. Commun. (2005) 2131.
[19] X. Zhang, F. Zhang, K.Y. Chan, Appl. Catal. A: Gen. 284 (2005) 193.
[20] H. Uchiyama, K. Suzuki, Y. Oaki, H. Imai, Mater. Sci. Eng. B 123 (2005) 248.
[21] E. Allain, S. Besson, C. Durand, M. Moreau, T. Gacoin, J.P. Boilot, Adv. Funct. Mater. 17 (2007) 549.
[22] M. Alvaro, C. Aprile, M. Benitez, E. Carbonell, H. Garcia, J. Phys. Chem. B 110 (2006) 6661.
[23] M. Kang, W.J. Hong, M.S. Park, Appl. Catal. B 53 (2004) 195.
[24] Y. Li, S. Kim, J. Phys. Chem. B 109 (2005) 12309.
[25] Y. Shiraishi, N. Saito, T. Hirai, J. Am. Chem. Soc. 127 (2005) 8304.
[26] Y. Shiraishi, N. Saito, T. Hirai, Chem. Commun. (2006) 773.
[27] Y. Shiraishi, D. Tsukamoto, T. Hirai, Org. Lett. 10 (2008) 3117.
[28] Y. Shiraishi, M. Morishita, T. Hirai, Chem. Commun. (2005) 5977.
[29] H. Koizumi, Y. Shiraishi, S. Tojo, M. Fujitsuka, T. Majima, T. Hirai, J. Am. Chem. Soc. 128 (2006) 8751.
[30] Y. Shiraishi, M. Morishita, Y. Teshima, T. Hirai, J. Phys. Chem. B 110 (2006) 6587.
[31] Y. Shiraishi, Y. Teshima, T. Hirai, Chem. Commun. (2005) 4569.
[32] Y. Shiraishi, Y. Teshima, T. Hirai, J. Phys. Chem. B 110 (2006) 6257.
[33] I.V. Tekto, V.Y. Tanchuk, T.N. Kasheva, A.E.P. Villa, J. Chem. Inf. Comput. Sci. 41 (2001) 1488.
[34] I.V. Tekto, V.Y. Tanchuk, J. Chem. Inf. Comput. Sci. 42 (2002) 1136.
[35] A. Cassez, A. Ponchel, F. Hapiot, E. Monflier, Org. Lett. 8 (2006) 4823.
[36] E.M. Sletten, C.R. Bertozzi, Org. Lett. 10 (2008) 3097.
[37] D. Lawless, N. Serpone, D. Meisel, J. Phys. Chem. 95 (1991) 5166.
[38] M. Suh, P.S. Bagus, S. Pak, M.P. Rosynek, J.H. Lunsford, J. Phys. Chem. B 104 (2000) 2736.
[39] M. Tokeshi, T. Minagawa, T. Kitamori, Anal. Chem. 72 (2000) 1711.
[40] V.M. Byakov, L.T. Bugaenko, E.A. Antonova, D.V. Paramonov, V.I. Trofimov, High Energy Chem. 34 (2000) 356.
[41] V. Brezova, P. Tarabek, D. Dvoranova, A. Stasko, S. Biskupic, J. Photochem. Photobiol. A: Chem. 155 (2003) 179.
[42] Y. Ohkuma, S. Kawanishi, Biochem. Biophys. Res. Commun. 257 (1999) 555.
[43] E.G. Janzen, D.E. Nutter Jr., E.R. Davis, B.J. Blackburn, J.L. Poyer, P.B. McCay, Can. J. Chem. 56 (1978) 2237.
[44] K. Hashimoto, T. Kawai, T. Sakata, J. Phys. Chem. 88 (1984) 4083.
[45] A. Sobczynski, L. Duczmal, W. Zmudzinski, J. Mol. Catal. A: Chem. 213 (2004) 225.
[46] M. Fujihira, Y. Satoh, T. Osa, J. Electroanal. Chem. 126 (1981) 277.
[47] I. Izumi, W.W. Dunn, K.O. Wilbourn, F.-R.F. Fan, A.J. Bard, J. Phys. Chem. 84 (1980) 3207.
[48] K.-I. Shimizu, H. Akahane, T. Kodama, Y. Kitayama, Appl. Catal. A: General 269 (2004) 75.
[49] K.-I. Shimizu, T. Kaneko, T. Fujishima, T. Kodama, H. Yoshida, Y. Kitayama, Appl. Catal. A: General 225 (2002) 185.
[50] J. Chen, L. Eberlein, C.H. Langford, J. Photochem. Photobiol. A: Chem. 148 (2002) 183.